

# Self-dual random-plaquette gauge model and the quantum toric code

Koujin Takeda\* and Hidetoshi Nishimori

Department of Physics, Tokyo Institute of Technology,  
Oh-okayama, Meguro, Tokyo 152-8551, Japan

## Abstract

We study the four-dimensional  $Z_2$  random-plaquette lattice gauge theory as a model of topological quantum memory, the toric code in particular. In this model, the procedure of quantum error correction works properly in the ordered (Higgs) phase, and phase boundary between the ordered (Higgs) and disordered (confinement) phases gives the accuracy threshold of error correction. Using self-duality of the model in conjunction with the replica method, we show that this model has exactly the same mathematical structure as that of the two-dimensional random-bond Ising model, which has been studied very extensively. This observation enables us to derive a conjecture on the exact location of the multicritical point (accuracy threshold) of the model,  $p_c = 0.889972 \dots$ , and leads to several nontrivial results including bounds on the accuracy threshold in three dimensions.

---

\*E-mail address: takeda@stat.phys.titech.ac.jp

# 1 Introduction

The lattice gauge theory has been studied mainly from the standpoint of particle physics. Many interesting results have been known for years for systems with spatially uniform couplings [1]. The lattice gauge theory with randomness in couplings has not been a target of active studies mainly due to lack of physical motivation. However, it was recently proposed that the random lattice gauge model can be related closely with error-correcting processes of the toric code, an interesting example of quantum information storage [2, 3, 4]. This observation serves as a strong motivation to investigate the random case systematically.

In Refs. [2, 3, 4], the two-dimensional ( $2D$ )  $\pm J$  random-bond Ising model (RBIM) and the  $3D$   $Z_2$  random-plaquette gauge model (RPGM) were studied in the context error corrections of the toric code. More precisely, the error-correcting processes of the bond-qubit model, where a qubit resides on each bond of the lattice, can be mapped to the RBIM. The plaquette-qubit model, where a qubit is located on each plaquette, is similarly related to the RPGM as far as error-corrections are concerned.

In the toric code, we assume that the phase error and bit flip error may occur on each qubit due to decoherence and interactions with the environment. Fortunately, if the number of errors is not very large, we can determine the “error chains” or “error sheets” from the measured syndrome, or the positions where check operators give nontrivial signs ( $-1$ ). We can then correct the errors by applying appropriate operators to the relevant error positions, and the encoded information, which is the simultaneous eigenstate of all check operators with trivial (unit) eigenvalues, is recovered. However, if the error rate becomes larger than a threshold (accuracy threshold), this procedure of error correction fails because nontrivial ambiguities arise in the error positions, and consequently the encoded information is lost. It is therefore very important to obtain the correct value of the accuracy threshold.

The corresponding statistical models such as the RBIM or the RPGM have two parameters: the temperature  $T$  and the probability  $1 - p$  for the interaction on a bond (plaquette) to be negative, which corresponds to the error rate in the context of toric code. The error-correcting properties of the toric code are related to the ordering behaviour of the RBIM/RPGM on a line in the  $p$ - $T$  plane (phase diagram). Error correction can be performed successfully in the magnetically ordered phase in the  $p$ - $T$  plane of the RBIM (RPGM), which means stable storage of the encoded information, while in the disordered phase error correction fails and the encoded information is lost. The transition point (the multicritical point on the Nishimori line [5]) is thus supposed to give the accuracy threshold of error correction. It is therefore crucial to know the correct location of the multicritical point of

these models for the design of reliable quantum storage, for example.

These recent results have lead us to the study of the  $4D$   $Z_2$  RPGM which can be related to the  $4D$  toric code. A part of the reasons to investigate the  $4D$  model, not  $2D$  or  $3D$  cases, is that the system with spatially uniform coupling is known to be self dual in  $4D$  [6], which serves as a powerful tool of analyses. In addition, the model of plaquette toric code on the  $3D$  cubic lattice under repeated measurement is also related to the  $4D$  RPGM. As has been mentioned above, the  $4D$  plaquette gauge model has a useful property of self duality, and we will analyze the  $4D$  RPGM using the duality technique. The formalism of duality transformation used in this paper is due to Wu and Wang [7]. They proposed the method of duality transformation using Fourier transformation for the analysis of  $2D$  non-random multi-component spin models. Recently it has been shown in Ref. [8] that the Wu-Wang duality is applicable to studying the  $2D$  *random* spin model. We show that the duality analysis developed in Ref. [8] is also applicable to the study of the  $4D$  RPGM. Our main conclusion is that the mathematical structure determining the multicritical point of the  $4D$  RPGM between the ordered (Higgs) and the disordered (confinement) phases is closely related to that of the  $2D$  RBIM, whose property has been studied extensively for years. This suggests that the accuracy threshold of the  $4D$  plaquette toric code coincides with the  $2D$  bond toric code. We also elucidate the correspondence between the  $4D$  plaquette qubit toric code and the  $4D$  RPGM.

The  $3D$  RPGM can be viewed as a model of the  $3D$  toric code as well. We also study the phase structure of the  $3D$  RPGM using the Wu-Wang duality and give useful bounds on the value of accuracy threshold of error correction.

This paper is organized as follows. In Sec. 2 we review the toric codes for the  $2D$  bond model and the  $4D$  plaquette model. We also elucidate the relation between the toric code and the random spin systems such as the RBIM and the RPGM. In Sec. 3 we explain the Wu-Wang duality technique using the  $2D$  Ising model on the square lattice, which is one of the simplest self-dual models. In Sec. 4 self-duality of the  $4D$  plaquette gauge model without randomness is explained. In Sec. 5 we incorporate randomness to the  $4D$  plaquette gauge model and analyze it using duality and the method of averaged Boltzmann factor in conjunction with the replica method proposed in Ref. [8]. In Sec. 6 the  $3D$  RPGM is investigated using its dual representation. In the dual space, the  $3D$  RPGM can be transformed to an  $n$ -replicated spin system with spatially uniform couplings. Relation to the  $3D$  toric code is also discussed. Section 7 is devoted to conclusion and discussions.

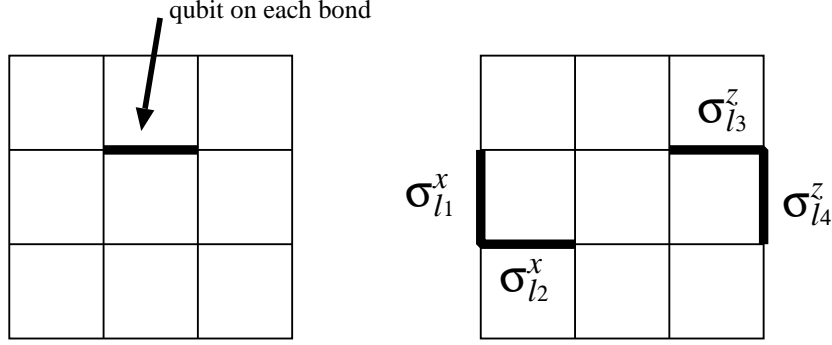


Figure 1: Qubits reside on bonds in the toric code (left). Possible error chains (right).

## 2 Toric code in $2D$ and $4D$

For clarity of presentation, let us first review the toric code for quantum error correction and its relation to spin and gauge models. The toric code is a method to encode quantum information for its stable storage using topological nontriviality of the manifold on which qubits are located.

It is useful to start with the  $2D$  toric code to explain the basic idea [2]. In this case the toric code is defined on the  $2D$  square lattice on the torus, and qubits reside on bonds (Fig. 1). We represent the two states of the qubit by 2-vector  $\begin{pmatrix} 1 \\ 0 \end{pmatrix}$  and  $\begin{pmatrix} 0 \\ 1 \end{pmatrix}$ . Any state of a specified bond can be expressed as a linear combination of these vectors. A quantum state of the whole system is given by the direct product of these states. The stored quantum information is chosen as a linear combination of such direct products which is a simultaneous eigenstate  $|\Psi\rangle$  of all check operators (to be defined below) with trivial eigenvalue 1.

This system suffers from errors caused by decoherence and interactions with the environment, and the errors change the states of qubits on bonds. There are two types of errors; one is a bit-flip error which flips the qubit to the other state, and the other is a phase error to change the phase of qubit. We express these errors by the operations of Pauli matrices to the original state. Existence of these errors on bond  $l$  is expressed as  $\sigma_l^x|\Psi\rangle$  (bit-flip error) and  $\sigma_l^z|\Psi\rangle$  (phase error). We can check if these errors have occurred by the operation of check operators. For this purpose, we define two kinds of check operators,

$$X_i = \bigotimes_{l \in \partial i} \sigma_l^x, \quad (1)$$

$$Z_P = \bigotimes_{l \in \partial P} \sigma_l^z, \quad (2)$$

where  $X_i$  is defined on each site and  $Z_P$  on each plaquette (shown on the left of Fig. 2). All check

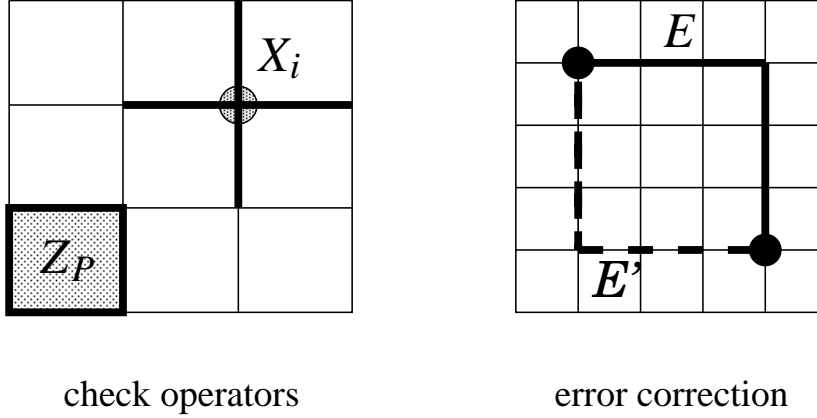


Figure 2: Check operators and the inference procedure of error chain. Black circles denote syndrome.

operators at any sites or plaquettes commute with each other,  $[X_i, Z_P] = 0$ , and hence simultaneous eigenstates of these check operators exist. The eigenvalues of these check operators are  $\pm 1$ . We may therefore choose the stored quantum state  $|\Psi\rangle$  as a simultaneous eigenstate of all these check operators with the eigenvalue 1.

Let us now consider the case that a chain of phase errors emerge. Bit-flip errors can be treated similarly on the dual lattice. We can detect the error chain by operating check operators to the stored quantum state. Phase error caused by  $\sigma_l^z$  can be detected by the check operator  $X_i$  on the original lattice and a chain of bit-flip errors (due to  $\sigma_l^x$ ) by the operator  $Z_P$  on the dual lattice. Since we prepare the original state whose eigenvalues of check operators are all positive (1), we can find the end positions of the error chain from the positions of a wrong sign ( $-1$ ) of check operators, called syndrome. It should be remembered here that we can detect only both ends of the error chain, and we are asked to infer the actual configuration of the chain from its ends. In some cases our inference of error chain is successful, while in other cases we might infer a wrong error chain. An example of error correction procedure is shown in Fig. 2 (right). We can detect only the ends (black circles, syndrome) of a real error chain ( $E$ ) as the sites where  $X_i|\Psi\rangle = -|\Psi\rangle$  in the case of phase errors. An example of correction chain inferred from the syndrome is shown dotted ( $E'$ ). The example shown in Fig. 2 is a case of successful correction, where two chains  $E$  and  $E'$  are different but homologically equivalent. The reason will be explained later.

In Fig. 3 are shown two examples of error correction. An example of successful correction is shown on the left. In this case, the real error chain ( $E$ , solid line) and correction chain ( $E'$ , dotted line) form a loop, which is homologically trivial (or can be shrunk to a point). Since the change of  $E$  to  $E'$  (or vice versa) is represented by the operators  $Z_P$  on the plaquettes inside the loop  $E + E'$

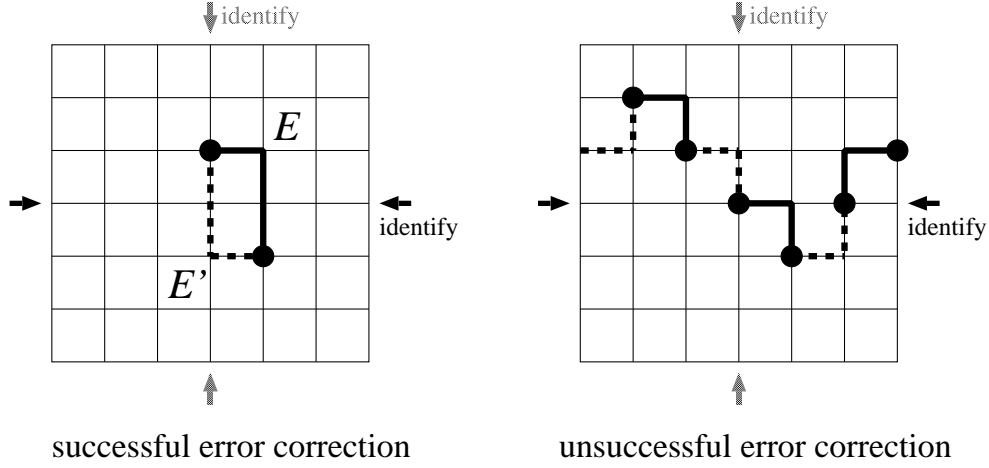


Figure 3: Successful and unsuccessful error corrections.

and  $|\Psi\rangle$  is invariant by their operation, the difference between  $E$  and  $E'$  is not essential,

$$\bigotimes_{l \in E} \sigma_l^z |\Psi\rangle = \bigotimes_{l \in E'} \sigma_l^z |\Psi\rangle. \quad (3)$$

An example on the right of Fig. 3 is an unsuccessful case. In this case,  $E$  and  $E'$  form a homologically nontrivial loop on the torus. It is impossible to change  $E$  to  $E'$  by operating  $Z_p$ 's. Thus an error correction by using  $E'$  (dotted lines) yields a different (erroneous) result. Such an unsuccessful correction procedure often occurs when the error rate becomes large because many/long error chains may exist. It is expected from these examples that the accuracy threshold of error correction exists.

Next we explain the relation between the 2D toric code and the 2D RBIM (Fig. 4) [3]. First let us consider the procedure of successful error correction when the real error chain  $E$  and correction chain  $E'$  constitute a homologically trivial loop. It is useful to consider the dual lattice. We assign a spin on each dual site and an interaction for each dual bond (Fig. 4, right). In doing so, we reverse spins inside the loop  $E + E'$  and assign antiferromagnetic (reversed sign) interactions to the bonds which correspond to the error chain  $E$ . By this procedure the 2D toric code can be seen as a  $(\pm J)$  RBIM. The error rate  $1 - p$  of the toric code corresponds to the probability of antiferromagnetic interaction for each bond. The ratio of error probability to non-error probability  $(1 - p)/p$  is identical with the edge Boltzmann factor of local interaction corresponding to the ratio of unfavourable and favourable spin alignment,  $e^{-K}/e^K$  as seen in Fig. 4. Thus the 2D RBIM under consideration lies on the Nishimori line defined by  $e^{-2K} = (1 - p)/p$  [5].

The relation between the phase diagram of the 2D RBIM and accuracy threshold of the toric code is explained intuitively as follows [3, 4]. In the magnetically ordered phase of the RBIM, error

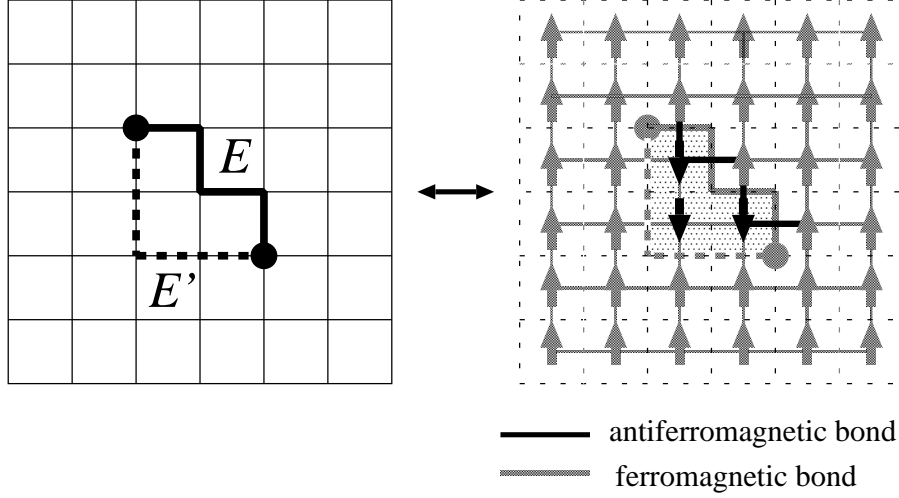


Figure 4: Correspondence between the toric code and the RBIM.

correction is successful since the islands of reversed spins as depicted on the right of Fig. 4 are not extensively large in the ordered phase, which implies that the difference between  $E$  and  $E'$  is not significant. On the other hand, in the disordered phase, the error correction fails and encoded information is lost. Thus the critical probability of antiferromagnetic bond at the phase boundary along the Nishimori line (multicritical point) gives the accuracy threshold of error correction in the toric code.

Now we generalize the toric code from the  $2D$  bond-qubit system to the  $4D$  plaquette-qubit system. A motivation is that the accuracy threshold of the  $4D$  plaquette-qubit system can be estimated from the study of the corresponding  $4D$  gauge model which can be analyzed by duality, as shown in the following sections. For this purpose we prepare a  $4D$  hypercubic lattice and assign a qubit on each plaquette (Fig. 5). Bit-flip and phase errors occur on each plaquette. We define the check operator as follows,

$$X_l = \bigotimes_{l \in \partial P} \sigma_P^x, \quad (4)$$

$$Z_C = \bigotimes_{P \in \partial C} \sigma_P^z, \quad (5)$$

where  $X_l$  is defined on each bond and  $Z_C$  on each  $3D$  cube on the  $4D$  lattice as shown in Fig. 5 (right). We can check a phase error  $\sigma_P^z$  by the operator  $X_l$  and a bit-flip error  $\sigma_P^x$  by  $Z_C$ . In the same way as in the  $2D$  case, the phase error  $\sigma_P^z$  is detected on the original lattice and the bit-flip error  $\sigma_P^x$  on the dual lattice. Note that the plaquette model on the  $4D$  hypercubic lattice is self-dual in the sense that the dual system also carries its degrees of freedom on plaquettes as elucidated

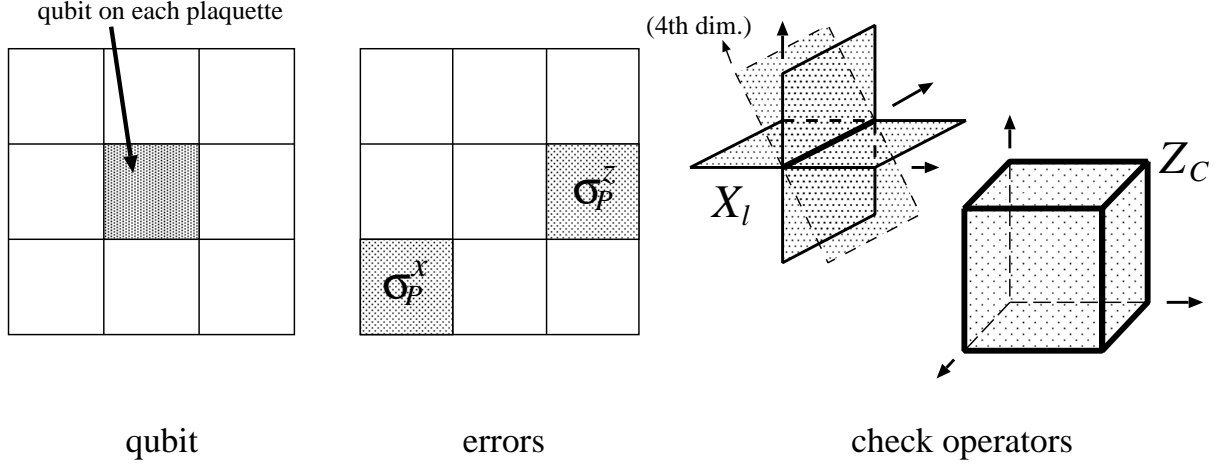


Figure 5: 4D toric code (I): Qubits errors and check operators are displayed. The 2D square lattice is a part of the 4D hypercubic lattice.

below.

Let us consider the correction procedure of phase errors (Fig. 6). An error chain in the 2D bond toric code becomes an “error sheet” in the present 4D case. We detect the error sheet using the check operator  $X_l$ . We can determine only the boundary of the error sheet from syndrome, which is similar to the 2D bond case. We must infer the error sheet itself from its boundary. In the correction procedure, the real error sheet  $E$  and the correction sheet  $E'$  form a connected surface. If the surface is closed or homologically trivial (middle in Fig. 6), error correction is successful because the operations of correcting operators on  $E$  and  $E'$  are equivalent to each other. On the other hand the correction procedure is not successful when the surface is homologically nontrivial (right in Fig. 6).

The correspondence of the 4D plaquette toric code and the 4D RPGM is similar to the 2D case [3]. Here we consider the case of successful error correction. Suppose that an error occurs with probability  $1 - p$  on each plaquette. The probability  $\text{Prob}(E, E')$  that the error sheet  $E$  and the correction sheet  $E'$  are generated is given by (similarly to Fig. 4),

$$\text{Prob}(E, E') \propto \prod_P \exp(K_P U_P), \quad (6)$$

where  $U_P$  takes  $-1$  on the surface  $C = E + E'$  and  $1$  elsewhere. Here  $K_P$  is defined by

$$e^{-2K_P} = \begin{cases} (1-p)/p, & \text{for } P \notin E, \\ p/(1-p), & \text{for } P \in E. \end{cases} \quad (7)$$



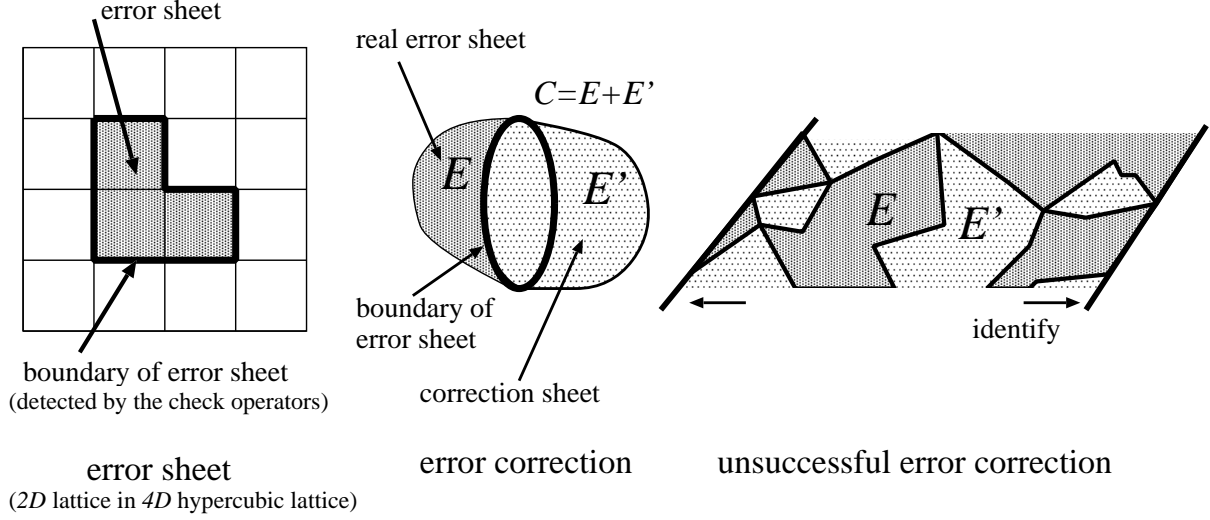


Figure 6: The 4D toric code (II): Error sheet and error correction procedure. The error sheet and correction sheet shown in the figure are hyperplanar surfaces.

For each bond  $l$  on the 4D lattice,  $U_P$  must satisfy the constraint (because a connected surface  $C$  has no boundary),

$$\prod_{P: l \in \partial P} U_P = 1, \quad (8)$$

or on the dual lattice,

$$\prod_{P': P' \in \partial C'} U_{P'} = 1, \quad (9)$$

for each dual cube  $C'$ . We introduce dual bond variables to solve this constraint,

$$U_{P'} (= U_P) = \prod_{l' \in \partial P'} \tilde{\xi}_{l'}, \quad (10)$$

where  $\tilde{\xi}_{l'}$  is an ordinary Ising variable which takes  $\pm 1$ . Using  $K_{P'} (= K_P)$  and  $U_{P'}$ , we can rewrite the probability of Eq. (6),

$$\text{Prob}(E, E') \propto \prod_{P'} \exp \left\{ K_{P'} U_{P'}(\tilde{\xi}_{l'}) \right\} = \exp \left\{ K \sum_{P'} \tau_{P'} U_{P'}(\tilde{\xi}_{l'}) \right\}, \quad (11)$$

where  $\tau_{P'} = K_{P'}/K$  takes  $\pm 1$ . If we take the sum over  $\tilde{\xi}_{l'}$ , This turns to the partition function of the 4D RPGM, which we will study in Sec. 5.  $K$  is defined by  $e^{-2K} = (1-p)/p$ , the condition of the Nishimori line [5].

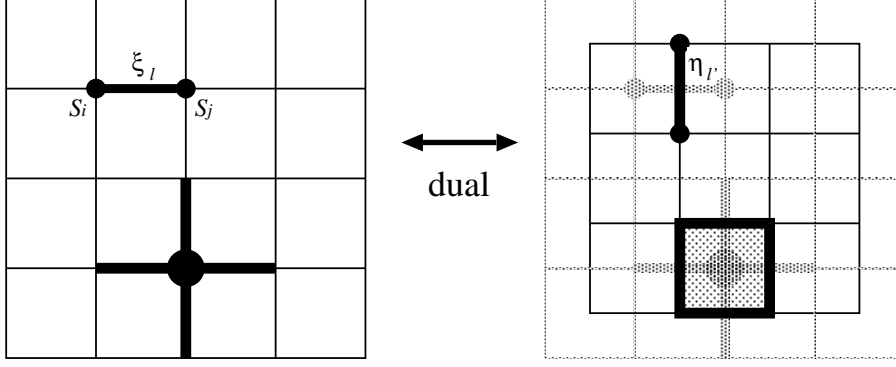


Figure 7: The 2D Ising model and its self-duality. Also illustrated is the derivation of modulo-2 Kronecker delta of Eq. (21) for each plaquette.

### 3 2D Ising model and Wu-Wang duality

The next step is to develop a framework to investigate the mathematical structure of the models defined in Sec. 2. We consider the 2D Ising model on the 2D square lattice in order to illustrate the powerful technique of Wu-Wang duality. The Hamiltonian of the Ising model is

$$H = -J \sum_{\langle ij \rangle} \tilde{S}_i \tilde{S}_j, \quad (12)$$

where  $\tilde{S}_i$  is the normal Ising spin variable which takes  $\pm 1$  and  $J$  is the uniform coupling constant. This Hamiltonian can be rewritten as,

$$H = J \sum_l \xi_l, \quad \xi_l = \sum_{i \in \partial l} S_i, \quad (13)$$

where  $l$  and  $i$  are bond and site, respectively, and  $S_i$  is the modulo-2 spin variable which takes 0 or 1 in this case. The summation over  $i$  in the definition of  $\xi_l$  is also defined by modulo 2. Note that a product of  $\tilde{S}_i$ 's has been changed to a sum of  $S_i$ 's.

The partition function is,

$$Z = \sum_{S_i=0,1} \prod_l u(\xi_l), \quad u(\xi_l) = \exp[-K \xi_l(S_i)], \quad (14)$$

where  $K = \beta J = J/kT$ . To take the dual of this model, we introduce a function obtained by regarding the modulo-2 bond variables  $\xi_l$  as independent variables in Eq. (14),

$$\tilde{Z} = \sum_{\xi_l=0,1} \prod_l u(\xi_l), \quad u(\xi_l) = \exp[-K \xi_l]. \quad (15)$$

Note that two functions Eqs. (14) and (15) do not coincide in their naive forms. To establish their equivalence, we must impose the following condition on the summation Eq. (15),

$$\sum_{l \in \partial P} \xi_l = 0 \pmod{2} \quad \text{for all } P, \quad (16)$$

where  $P$  is a plaquette on the  $2D$  square lattice, because  $\xi_l$  is composed of the modulo-2 sum of two  $S_i$ 's at the ends of  $l$ . This means that change of the value of spin  $S_i$  at an arbitrary site on a  $2D$  plaquette always causes modification two of the four  $\xi_l$ 's in the plaquette, and l.h.s. of Eq. (16) for any plaquette remains zero modulo 2. We denote the summation with this condition by a prime. For Eq. (15),

$$Z(u) = \text{const.} \times \sum'_{\xi_l=0,1} \prod_l u(\xi_l), \quad (17)$$

and we may then identify the two  $Z$ 's in Eqs. (14) and (17).

The dual representation of the partition function is derived as follows. The dual of a bond  $l$  ( $1D$  object) on the  $2D$  square lattice is also a bond  $l'$  (Fig. 7). We define the dual bond variables  $\eta_{l'}$  on the dual lattice, which also take the value 0 or 1, and perform a discrete Fourier transformation of  $u(\xi_l)$  defined by

$$u^*(\eta_{l'}) = \frac{1}{\sqrt{2}} \sum_{\xi_l=0,1} \exp(\pi i \xi_l \eta_{l'}) u(\xi_l) = \frac{1}{\sqrt{2}} \sum_{\xi_l=0,1} \exp\left(\pi i \left(\sum_{i \in \partial l} S_i\right) \eta_{l'}\right) u(\xi_l), \quad (18)$$

or conversely,

$$u(\xi_l) = \frac{1}{\sqrt{2}} \sum_{\eta_{l'}=0,1} \exp\left(\pi i \left(\sum_{i \in \partial l} S_i\right) \eta_{l'}\right) u^*(\eta_{l'}). \quad (19)$$

More explicitly, the edge Boltzmann factors are,

$$\begin{aligned} u(0) &= 1, \\ u(1) &= e^{-K}, \\ u^*(0) &= \frac{1}{\sqrt{2}}(1 + e^{-K}), \\ u^*(1) &= \frac{1}{\sqrt{2}}(1 - e^{-K}). \end{aligned} \quad (20)$$

We use Eq. (19) in Eq. (14) and take the sums over  $S_i$ . Considering that a single site always appears at the ends of four bonds on the  $2D$  square lattice, the exponential factors in Fourier transformation lead (modulo-2) to Kronecker deltas such as,

$$\delta_{\text{mod } 2} \left( \sum_{l' \in \partial P'} \eta_{l'} \right) \quad \text{for all } P', \quad (21)$$

where  $P'$  is the dual plaquette on the  $2D$  dual square lattice (Fig.7). This condition is equivalent to Eq. (16) and we can replace the summation over  $\eta_{l'}$  with the constrained one.

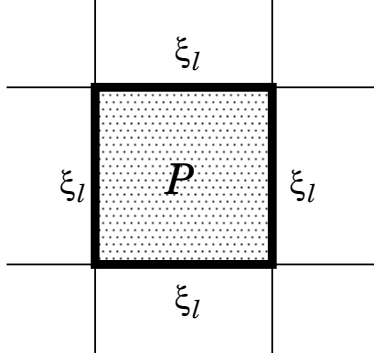


Figure 8: Bond variables and a plaquette.

Now we can express the partition function using dual variables,

$$Z(u^*) = \text{const.} \times \sum_{\eta_{l'}=0,1} \prod_{l'} u^*(\eta_{l'}). \quad (22)$$

We have therefore obtained a direct relation between the two partition functions in Eqs. (17) and (22),

$$Z(u) = \text{const.} \times Z(u^*). \quad (23)$$

The transition point, if unique, is identified with the fixed point of duality transformation of the edge Boltzmann factor,

$$u(0) = u^*(0), \quad u(1) = u^*(1), \quad (24)$$

both of which lead to the same relation<sup>1</sup>

$$e^{-K_c} = \sqrt{2} - 1. \quad (25)$$

## 4 4D $Z_2$ lattice gauge model and Wu-Wang duality

Let us move on to the 4D  $Z_2$  gauge model. We can treat this model using duality in an analogous manner to the 2D Ising model. The Hamiltonian is

$$H = J \sum_P U_P, \quad U_P = \sum_{l \in \partial P} \xi_l \quad (\simeq - \prod_{l \in \partial P} \tilde{\xi}_l), \quad (26)$$

where  $P$  and  $l$  are the plaquette and bond on the 4D hypercubic lattice, respectively (Fig. 8), and  $J$  is the uniform coupling constant. Here  $\xi_l$  is the modulo-2 variable which takes 0 or 1 and the

---

<sup>1</sup>If we start with the Hamiltonian Eq.(12), the transition point will be given by the relation  $e^{-2K_c} = \sqrt{2} - 1$ . This difference is caused by the definitions of the coupling  $J$  in Eqs. (12) and (13), which differ by factor 2.

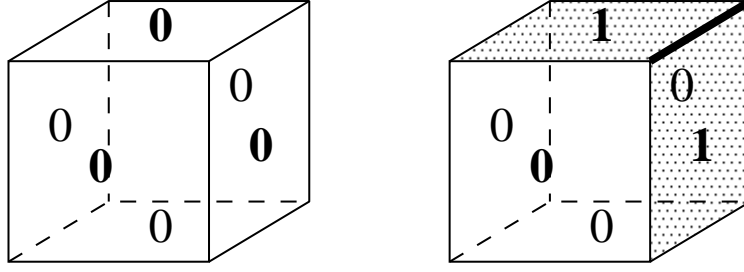


Figure 9: Illustration of the condition Eq. (29): A 3D cube and  $U_P$ 's of six faces are shown. The operation of changing  $\xi_l$  for one edge (shown in a thick line) always induces the changes of two  $U_P$ 's.

sum over  $l$  is also defined by modulo 2. ( $\tilde{\xi}_l$  is the ordinary Ising spin variable which takes  $\pm 1$ .) The partition function is,

$$Z = \sum_{\xi_l=0,1} \prod_P u(U_P), \quad u(U_P) = \exp[-KU_P(\xi_l)]. \quad (27)$$

To take the dual, we regard  $U_P$  as the independent plaquette variables,

$$\tilde{Z} = \sum_{U_P=0,1} \prod_P u(U_P), \quad u(U_P) = \exp[-KU_P]. \quad (28)$$

Functions (27) and (28) do not necessarily coincide unless we impose the following condition on the summation Eq. (28),

$$\sum_{P \in \partial C} U_P = 0 \pmod{2} \quad \text{for all } C, \quad (29)$$

where  $C$  is a 3D cube on the 4D hypercubic lattice. This means that, if we change the value of  $\xi_l$  at an arbitrary edge of the 3D cube, two of six  $U_P$ 's on the faces automatically change, and l.h.s. of Eq. (29) for any cube remains zero modulo 2 (Fig. 9). We denote the summation with this condition with a prime. For Eq. (28),

$$Z(u) = \text{const.} \times \sum'_{U_P=0,1} \prod_P u(U_P). \quad (30)$$

This expression is identified with Eq. (27).

Next we represent the partition function in the dual form. The dual of a plaquette  $P$  (2D object) on the 4D hypercubic lattice is also a plaquette  $P'$ . We define the variables  $V_{P'}$  on dual plaquettes, which also take the value 0 or 1, and perform a Fourier transformation of  $u(U_P)$ ,

$$u^*(V_{P'}) = \frac{1}{\sqrt{2}} \sum_{U_P=0,1} \exp(\pi i U_P V_{P'}) u(U_P) = \frac{1}{\sqrt{2}} \sum_{U_P=0,1} \exp\left(\pi i \left(\sum_{l \in \partial P} \xi_l\right) V_{P'}\right) u(U_P), \quad (31)$$

or conversely,

$$u(U_P) = \frac{1}{\sqrt{2}} \sum_{V_{P'}=0,1} \exp\left(\pi i \left(\sum_{l \in \partial P} \xi_l\right) V_{P'}\right) u^*(V_{P'}). \quad (32)$$

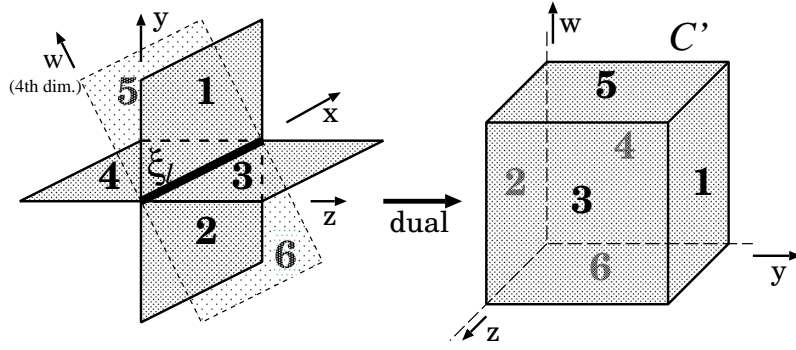


Figure 10: Illustration of the condition Eq. (33) in the dual space: 3D cube in the dual space is localized in the  $x$  direction.

We insert Eq. (32) into Eq. (27) and take the sums over  $\xi_l$ . Considering that a bond is always at the boundaries of six faces, the exponential factors in the Fourier transformation yield deltas (modulo-2) such as,

$$\delta_{\text{mod } 2} \left( \sum_{P' \in \partial C'} V_{P'} \right) \quad \text{for all } C', \quad (33)$$

where  $C'$  is the dual cube on the 4D dual hypercubic lattice (Fig. 10). This condition is equivalent to Eq. (29) and we can replace the summation over  $V_{P'}$  with the constrained one.

We have thus obtained the partition function using the dual variables,

$$Z(u^*) = \text{const.} \times \sum_{V_{P'=0,1}}' \prod_{P'} u^*(V_{P'}). \quad (34)$$

The two partition functions in Eqs. (30) and (34) are related as,

$$Z(u) = \text{const.} \times Z(u^*). \quad (35)$$

From this relation, we can derive the transition point as in the 2D case,

$$e^{-K_c} = \sqrt{2} - 1, \quad (36)$$

which is equivalent to the one of the 2D Ising model Eq.(25).

## 5 4D random plaquette gauge theory

Next we explain the technique of dual transformation to deal with the RPGM following Ref. [8]. They studied the 2D ( $\pm J$ ) RBIM mainly using the Wu-Wang duality. Our method for analyzing the 4D RPGM is essentially the same as in Ref. [8].

From the motivation related to quantum error correction explained in Sec. 2, we incorporate randomness in the plaquette gauge model Eq. (26),

$$H = J \sum_P \tau_P U_P, \quad (37)$$

where  $\tau_P$  is a plaquette-dependent quenched random variable. Here we assume that  $\tau_P$  takes 1 with probability  $p$  and  $-1$  with  $1 - p$ .

We make use of the replica technique for averaging over randomness in  $\tau_P$ . That is, we prepare  $n$  replica systems and take the  $n \rightarrow 0$  limit in the end to obtain physical quantities. After the configuration average over random plaquette variables, the partition function is determined by local non-random plaquette Boltzmann factors because the system then acquires spatial homogeneity. In the following we define the “averaged” plaquette Boltzmann factor for a given probability  $p$ .

First we consider the simplest case of  $n = 1$ . We define the plaquette Boltzmann matrix<sup>2</sup> as

$$p \begin{bmatrix} \kappa_+ & \kappa_- \\ \kappa_- & \kappa_+ \end{bmatrix} + (1 - p) \begin{bmatrix} \kappa_- & \kappa_+ \\ \kappa_+ & \kappa_- \end{bmatrix} \equiv \begin{bmatrix} x_0 & x_1 \\ x_1 & x_0 \end{bmatrix} = A_1, \quad (38)$$

where  $\kappa_{\pm} = e^{\pm K}$ .  $x_0$  means the averaged Boltzmann factor for the configuration  $\prod_l U_l = 1$  and  $x_1$  for  $\prod_l U_l = -1$ . For a generic  $n$ , we can obtain the  $2^n \times 2^n$  matrix  $A_n$  by a recursive procedure,

$$p \begin{bmatrix} \kappa_+ & \kappa_- \\ \kappa_- & \kappa_+ \end{bmatrix}^{\otimes n} + (1 - p) \begin{bmatrix} \kappa_- & \kappa_+ \\ \kappa_+ & \kappa_- \end{bmatrix}^{\otimes n} \equiv A_n = \begin{bmatrix} A_{n-1} & B_{n-1} \\ B_{n-1} & A_{n-1} \end{bmatrix}, \quad (39)$$

where  $B_n$  is obtained from  $A_n$  by replacing  $x_k \rightarrow x_{k+1}$ . The factor  $x_k$  is defined by generalizing  $x_0$  and  $x_1$  in Eq. (38) and corresponds to the averaged plaquette Boltzmann factor for the configuration  $\prod_l U_l = 1$  in  $n - k$  replicas and  $-1$  in  $k$  replicas. The explicit form of  $x_k$  is

$$x_k = p \kappa_+^{n-k} \kappa_-^k + (1 - p) \kappa_+^k \kappa_-^{n-k}. \quad (40)$$

The averaged partition function depends on averaged plaquette Boltzmann factors  $x_k$ ,

$$[Z^n]_{\text{av}} \equiv Z_n(x_0, x_1, \dots, x_n), \quad (41)$$

where  $[\ ]_{\text{av}}$  means random average.

On the dual lattice, we can also define the dual averaged plaquette Boltzmann factor  $x_k^*$  similarly. The Boltzmann factors for the original and dual systems are related by Eq. (31), and accordingly the relations between  $x_k$  and  $x_k^*$  for  $n = 1$  are given by replacing  $u$  and  $u^*$  with  $x$  and  $x^*$  respectively,

$$\begin{aligned} \sqrt{2}x_0^* &= x_0 + x_1, \\ \sqrt{2}x_1^* &= x_0 - x_1. \end{aligned} \quad (42)$$

---

<sup>2</sup>In this section and Sec. 6 we define the Boltzmann factor by the normal Ising spin variable  $\tilde{\xi}_l$  in Eq. (26) instead of the modulo-2 variable  $\xi_l$  in order to follow the notation of Ref. [8].

For  $n = 2$ ,

$$\begin{aligned} 2x_0^* &= (x_0 + x_1) + (x_1 + x_2) = x_0 + 2x_1 + x_2, \\ 2x_1^* &= (x_0 - x_1) + (x_1 - x_2) = x_0 - x_2, \\ 2x_2^* &= (x_0 - x_1) - (x_1 - x_2) = x_0 - 2x_1 + x_2, \end{aligned} \quad (43)$$

similarly to the  $2D$  case [8].

In a similar way, we can obtain the explicit form of  $x_k^*$  for  $n$  replicas,

$$\begin{aligned} 2^{n/2} x_{2m}^* &= (\kappa_+ + \kappa_-)^{n-2m} (\kappa_+ - \kappa_-)^{2m}, \\ 2^{n/2} x_{2m+1}^* &= (2p - 1) (\kappa_+ + \kappa_-)^{n-2m-1} (\kappa_+ - \kappa_-)^{2m+1}. \end{aligned} \quad (44)$$

We can write the duality of the partition function using  $x_k$  and  $x_k^*$ ,

$$Z_n(x_0, x_1, \dots, x_n) = Z_n(x_0^*, x_1^*, \dots, x_n^*), \quad (45)$$

where we have neglected the trivial factor in Eq. (35) which is irrelevant to thermodynamic properties.

This procedure is completely the same as in the  $2D$  RBIM. In the  $2D$  RBIM, the multicritical point on the Nishimori line defined by

$$e^{-2K} = \frac{1-p}{p}, \quad (46)$$

is supposed to give the lower bound of the probability  $p$  for ferromagnetic (ordered) phase. In Ref. [8], they conjectured that the phase boundary on the Nishimori line coincides with the crossing point of Eq. (46) and a line defined by the relation for the averaged Boltzmann factor,

$$x_0 = x_0^*. \quad (47)$$

They confirmed that this relation together with the condition of Eq. (46) leads to the exact multicritical point at least in the case of small and infinite  $n$ .

We write Eq. (47) explicitly with inverse temperature  $K$  and probability  $p$ ,

$$pe^{nK} + (1-p)e^{-nK} = 2^{-n/2}(e^K + e^{-K})^n. \quad (48)$$

In conjunction with the Nishimori relation Eq. (46), this yields,

$$p_c^{n+1} + (1-p_c)^{n+1} = 2^{-n/2}, \quad (49)$$

where  $p_c$  is the probability at the critical point on the Nishimori line (Fig. 11). If we expand Eq. (49) with respect to  $n$  and take the  $n \rightarrow 0$  limit, we obtain the relation of order  $O(n^1)$  terms,

$$-p_c \log p_c - (1-p_c) \log(1-p_c) = \frac{\log 2}{2}. \quad (50)$$



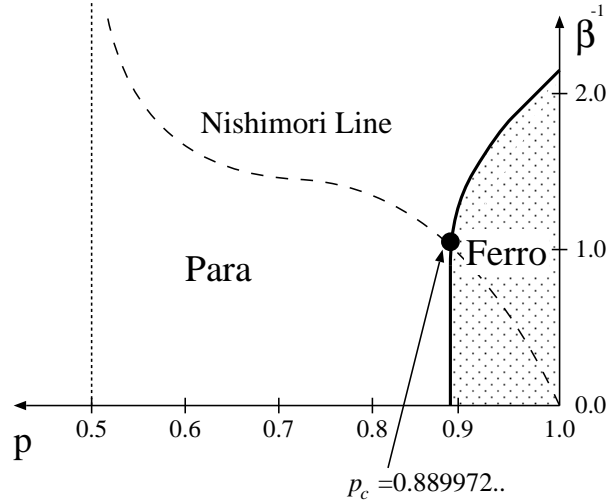


Figure 11: Phase diagram of the  $2D \pm J$  RBIM

This equation gives  $p_c = 0.889972 \dots$  numerically, which is in good agreement with the numerical studies in Ref. [9].

This argument for the  $2D$  RBIM is also applicable to the  $4D$  RPGM. In this latter model the order parameter is defined by the Wilson loop operator,

$$W[C] = \prod_{l \in C} \tilde{\xi}_l, \quad (51)$$

where  $C$  is an arbitrary closed loop. The random and thermal averaged value of  $W[C]$  obeys,

$$\ln([W[C]]_{\text{av},K}) \propto \begin{cases} [\text{length of } C] & \text{(perimeter law)} \\ & \text{for ordered (Higgs) phase,} \\ [\text{area of } C] & \text{(area law)} \\ & \text{for disordered (confinement) phase,} \end{cases} \quad (52)$$

where  $[ ]_{\text{av},K}$  means random and thermal averaged quantity. Higgs (ordered) and confinement (disordered) phases correspond to ferromagnetic and paramagnetic phase, respectively. If we apply the previous discussion for the  $2D$  RBIM to the  $4D$  RPGM, we automatically obtain the phase diagram for the  $4D$  RPGM from the one for the  $2D$  RBIM by replacing the names of phases. The transition probability at the critical point on the Nishimori line is also given by Eq. (50). We therefore conjecture that  $p_c = 0.889972 \dots$  satisfying Eq. (50) is the exact accuracy threshold of the  $4D$  plaquette toric code corresponding to the  $4D$  RPGM.

## 6 3D RPGM and dual representation

In this section we analyze the dual Boltzmann factor for the 3D RPGM and its representation by a spin model with ferromagnetic interactions. The discussion follows Ref. [8] where they mainly treated the 2D replicated  $\pm J$  Ising model.

We consider the  $\pm J$  RPGM with the Hamiltonian

$$H = -J \sum_P \tau_P U_P, \quad (53)$$

on the  $n$ -replicated 3D cubic lattice. The probability distribution of  $\tau_p$  is the same as in the previous section. The averaged Boltzmann factors  $x_k$  and the dual averaged Boltzmann factors  $x_k^*$  are defined similarly to Sec. 5. It should be remembered, however, that the interpretation of dual Boltzmann factor is different in this case; In the 3D system the plaquette model is not self-dual (that is, the duality relation of the partition function in Eq. (45) does not hold), and the dual of a plaquette (2D object) is a bond (1D object) as illustrated in Fig. 12. If we consider the averaged Boltzmann factor  $x_k$  on a plaquette on the original lattice, its dual Boltzmann factor  $x_k^*$  for a dual bond  $l^*$  is defined for the configuration  $S_i^* S_j^* = 1$  ( $S_i^*$  is a dual spin variable and  $i, j \in \partial l^*$ ) in  $n - k$  replicas and  $S_i^* S_j^* = -1$  in the remaining  $k$  replicas.

It is instructive to take the ratio of dual Boltzmann factors to  $x_0^*$ ,

$$\begin{aligned} x_{2m-1}^*/x_0^* &= (2p-1) \left( \frac{\kappa_+ - \kappa_-}{\kappa_+ + \kappa_-} \right)^{2m-1} = (2p-1) \tanh^{2m-1} K, \\ x_{2m}^*/x_0^* &= \tanh^{2m} K. \end{aligned} \quad (54)$$

This ratio can be written in the simple form

$$\exp\{K^*(S^{*(1)} + S^{*(2)} + \dots + S^{*(n)}) + K_p^* S^{*(1)} S^{*(2)} \dots S^{*(n)}\} \equiv Z_n(K, K_p), \quad (55)$$

where  $\tanh K = e^{-2K^*}$  and  $2p-1 = e^{-2K_p^*} (\equiv \tanh K_p)$ .  $S^{*(k)}$  is the Ising interaction factor in the  $k$ th replica,

$$S^{*(k)} = S_i^{*(k)} S_j^{*(k)} \quad (i, j \in \partial l^*). \quad (56)$$

From the Boltzmann factor Eq.(55), the dual model can be interpreted as a spin model which has ferromagnetic Ising interactions in each replica and an interaction between replicas.

Next we take the  $K_p^* \rightarrow \infty$  ( $K_p \rightarrow 0$ ) limit which corresponds to the  $p = 1/2$  case. In this case  $x_{2m-1}^*/x_0^*$  are zero for any  $m$  and  $S^{*(1)} S^{*(2)} S^{*(3)} \dots S^{*(n)}$  is unity. Therefore a spin variable can be removed by the relation  $S^{*(n)} = S^{*(1)} S^{*(2)} \dots S^{*(n-1)}$  and the dual Boltzmann factor becomes

$$Z_n(K, K_p = 0)$$

$$\begin{aligned}
&= A \exp\{K^*(S^{*(1)} + S^{*(2)} + \dots + S^{*(n-1)} + S^{*(1)}S^{*(2)} \dots S^{*(n-1)})\} \\
&= Z_{n-1}(K, K_p = K).
\end{aligned} \tag{57}$$

Thus the  $n$ -replicated system with  $K_p = 0$  ( $p = 1/2$ ) is equivalent to the  $(n-1)$ -replicated system with  $K = K_p$  (on the Nishimori line). The Boltzmann factor Eq. (55) includes only ferromagnetic interactions and the Griffiths inequality [10] holds, which leads to monotonicity of order parameters with respect to the change of  $K$  and  $K_p$  ( $T$  and  $p$ ). In particular the phase boundary between ferromagnetic and non-ferromagnetic phases is found to be a monotonic function of  $T$  and  $p$  (which are the parameters of the original model(=3D RPGM)). This fact yields,

$$T_c^n(p = 1/2) (= T_c^{n-1}(\text{MCP})) \leq T_c^n(\text{MCP}), \tag{58}$$

where  $T_c^n$  is the critical temperature for the  $n$ -replicated system and MCP means the multicritical point. We rewrite this inequality using probability  $p$ ,

$$p_c^{n-1}(\text{MCP}) \geq p_c^n(\text{MCP}), \tag{59}$$

where  $p_c^n$  is the probability of the multicritical point for the  $n$ -replicated system. Let us suppose that this inequality holds in the  $n \rightarrow 0$  limit. If we consider the  $n = 1$  system on the Nishimori line ( $K^* = K_p^*$ ), the dual Boltzmann factor becomes,

$$Z_1(K, K_p = K) = A \exp\{2K^*S^{*(1)}\}. \tag{60}$$

This is the simple ferromagnetic Ising Boltzmann factor and we can make use of the knowledge of the 3D ferromagnetic Ising model for the analysis. The critical point of the 3D non-random ferromagnetic Ising model is estimated as  $2K^* \simeq 0.22165 \dots$  numerically [11]. Using the condition ( $K = K^*$ ) and the dual relation ( $2p - 1 = e^{-2K_p^*}$ ), we obtain the value  $p_c^1(\text{MCP}) \simeq 0.9006$ . Finally we obtain the following inequality,

$$p_c^0(\text{MCP}) \geq p_c^1(\text{MCP}) \simeq 0.9006. \tag{61}$$

This inequality gives a lower bound of probability at the multicritical point for the 3D RPGM under the assumption that the inequality holds in the limit  $n \rightarrow 0$ .

The 3D RPGM is related to the toric code as well. We consider the toric code on the 3D cubic lattice and locate a qubit on each bond. If we choose check operators for this system as shown in Fig.12 (bond case), the accuracy threshold of *phase* error correction is given by the probability at phase boundary (on the Nishimori line) in the 3D RPGM. The accuracy threshold of *bit-flip* error correction is given by the phase boundary in the 3D RBIM. On the other hand, if we locate a qubit

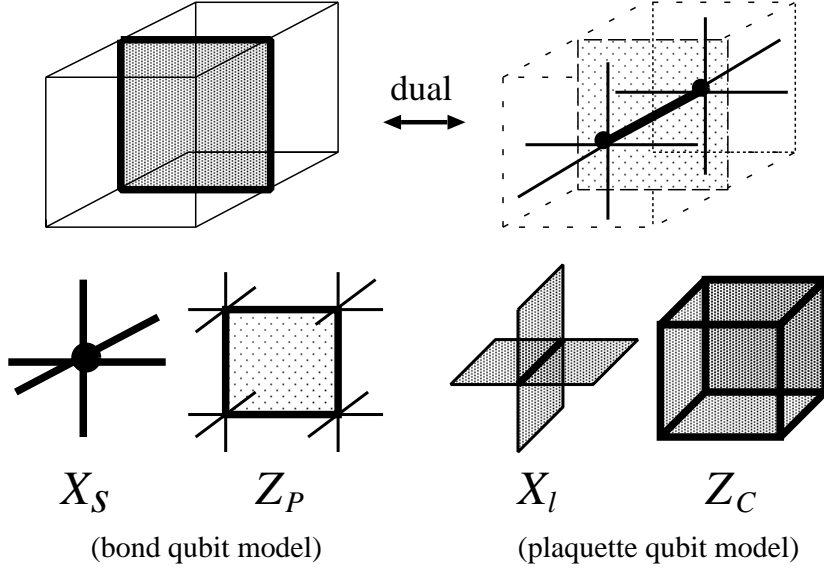


Figure 12: Duality of the 3D cubic lattice and check operators:  $X_s(X_l)$  is given by the product of Pauli matrix  $\sigma_x$  for each bond (plaquette).  $Z_P(Z_C)$  is given by the product of  $\sigma_z$  in the same way.

on each plaquette and choose the check operators like in Fig. 12 (plaquette case), the accuracy threshold of *bit-flip* error correction is given by the probability at phase boundary (on the Nishimori line) in the 3D RPGM. Similarly, the accuracy threshold of *phase* error correction is given by the critical point in the 3D RBIM. From this correspondence, we easily find out that the procedure of phase error correction in the 3D bond qubit system and that of bit-flip error correction in the 3D plaquette qubit system are related by duality. In the same way, the bit-flip error correction in the 3D bond system and phase error correction in the 3D plaquette system are dual to each other.

## 7 Conclusion and discussion

We have discussed the phase structure of the 4D RPGM using the method of duality and averaged Boltzmann factor. We have derived an equation to determine the location of the multicritical point (the accuracy threshold in the context of quantum error correction), which is expected to be exact (but is a conjecture, rigorously speaking). The structure of duality relations and the resulting equation for the multicritical point coincide precisely with the corresponding ones for the 2D RBIM. We could therefore generalize the generic duality relation originally proposed by Wegner [6] for non-random systems to the random case. In particular, the present argument can be extended to the model with  $n$ -dimensional objects in the  $2n$ -dimensional lattice. The same result will be able to be

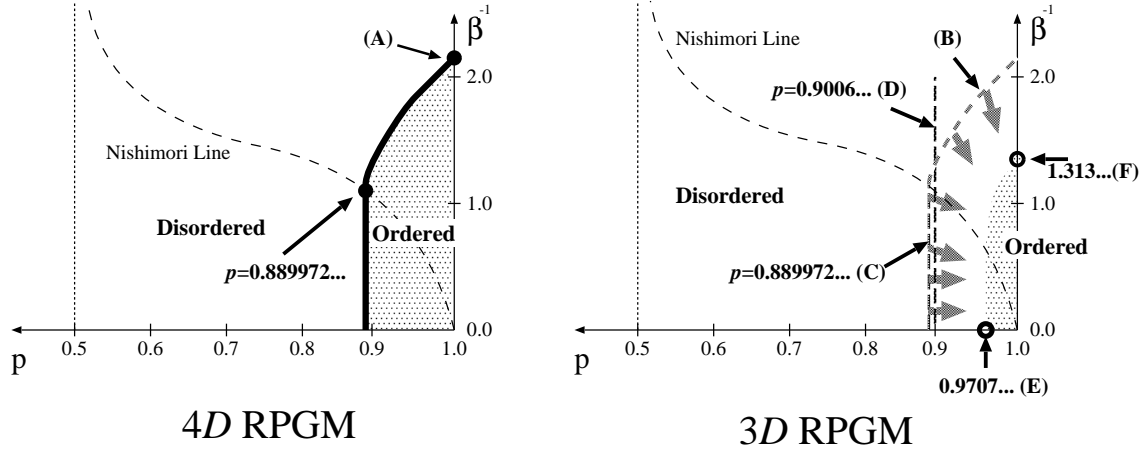


Figure 13: Phase diagram of the 4D and the 3D  $\pm J$  RPGM. Point (A): Critical point of non-random system obtained exactly from the duality of non-random model. Line (B): Phase boundary of the 4D RPGM. Line (C): Lower bound of  $p$  from the analysis of the 4D RPGM. Line (D): Lower bound of  $p$  from the analysis of the dual model of the 3D RPGM in Sec .6. Point (E): Critical point at  $T = 0$  by the numerical study in Ref. [4]. Point (F): Critical point of the non-random model obtained by the numerical study of the 3D Ising model and by the duality between the 3D Ising model and the 3D plaquette gauge model.

derived for these models.

We have elucidated the equivalence between the 4D RPGM and the 4D plaquette qubit toric code (and similarly for the 3D plaquette system). The phase boundary between the ordered and disordered phases on the Nishimori line gives the accuracy threshold of the toric code. From our study of the 4D RPGM, the accuracy threshold of the toric code with qubits on 4D plaquettes is expected to be given as  $p = 0.889972\dots$ , the same result as that of the 2D bond qubit system.

We may also expect that the phase boundary of the 4D RPGM gives a limit to the boundary of the ordered phase for the 3D RPGM (Fig. 13) because the reduction of dimension always enhances disorder. Of course the phase boundary of the 4D RPGM gives the lower bound of probability of ferromagnetic phase for the 3D RPGM ( $p = 0.889972\dots$ ). The lower bound was also estimated from the 3D Ising model using duality. The Griffiths inequality gives the lower bound  $p = 0.9006\dots$  on the assumption that the inequality holds for  $n \rightarrow 0$  limit. This is a better bound than the one from the study of the 4D RPGM ( $p = 0.889972\dots$ ). The transition point at  $T = 0$  (which is expected as the probability at the multicritical point) is estimated at  $p = 0.9707 \pm 0.0002$  in Ref. [4] by a numerical study, which is consistent with our inequality.

As for the  $4D$  plaquette toric code, a *local* error correction procedure is also proposed in Ref. [3]. The method is to be contrasted with that in the present paper where we use *global* information to infer the error positions because one needs the information of the boundary of error sheet. The difference between these correction procedures is as follows. Global procedure needs processes of fast classical computation to infer the real error sheet from its boundary, while the local procedure does not require such a classical computation because the local procedure needs only the local information of defects to remove all error sheets. On the other hand, the global procedure involves only a single observation to infer the error sheets and to correct errors. (Of course the observational errors occur in actual procedure and we must take them into consideration.) The local procedure requires many-step observations to erase all error sheets completely: The single correction step reduces the area of error sheet, but not to wipe them out at once. At the same time, we must notice that new error sheets may be generated during this process. If the rate of error generation is larger than the error reduction rate of the correction procedure, the error correction will fail because homologically nontrivial error sheet will be formed by the accumulation of error sheets, which affects the encoded information. (Remember that the homologically nontrivial sheet is formed by real error sheets and correction sheets in the global procedure.) Therefore the accuracy threshold also exists in the local procedure. In Ref. [3] an upper bound of accuracy threshold of the error correction by the local procedure is estimated from the argument mentioned above,  $p_c \simeq 1 - (4.8 \times 10^{-4})$ . As pointed out in Ref. [3], the local correction procedure cannot be applied to the bond-qubit system. We need at least four dimensions in order to perform the local correction procedure both for phase and bit-flip errors.

## Acknowledgement

The authors would like to thank Y. Ozeki, T. Sasamoto and T. Hamasaki for useful comments. This work was supported by the Grant-in-Aid for Scientific Research on Priority Area “Statistical-Mechanical Approach to Probabilistic Information Processing”.

## References

- [1] See e.g. C. Itzykson and J. -M. Drouffe, *Statistical Field Theory* (Cambridge University Press, Cambridge, 1989) and references therein.
- [2] A. Yu. Kitaev, “Quantum error correction with imperfect gates” in *Proceedings of the Third International Conference on Quantum Communication and Measurement*, edited by O. Hirota,

- A. S. Holevo and C. M. Caves (Plenum, New York, 1997); A. Yu. Kitaev, *Ann. Phys.* **303** (2003) 2.
- [3] E. Dennis, A. Kitaev, A. Landahl and J. Preskill, *J. Math. Phys.* **43** (2002) 4452.
- [4] C. Wang, J. Harrington and J. Preskill, *Ann. Phys.* **303** (2003) 31;  
Recently new results are obtained for 3D RPGM: G. Arakawa, I. Ichinose, *Ann. Phys.* **311** (2004) 152; T. Ohno, G. Arakawa, I. Ichinose, T. Matsui, quant-ph/0401101.
- [5] H. Nishimori, *Prog. Theor. Phys.* **66** (1981) 1169; H. Nishimori, *Statistical Physics of Spin Glasses and Information Processing: An Introduction* (Oxford University Press, Oxford, 2001).
- [6] F. J. Wegner, *J. Math. Phys.* **12** (1971) 2259; R. Balian, J. M. Drouffe and C. Itzykson, *Phys. Rev.* **D11** (1975) 2098; C. P. Korthals Altes, *Nucl. Phys.* **B142** (1978) 315; A. Ukawa, P. Windey and A. H. Guth, *Phys. Rev.* **D21** (1980) 1013.
- [7] F. Y. Wu and Y. K. Wang, *J. Math. Phys.* **17** (1976) 439.
- [8] J. -M. Maillard, K. Nemoto and H. Nishimori, *J. Phys.* **A36** (2003) 9799; H. Nishimori and K. Nemoto, *J. Phys. Soc. Jpn.* **71** (2002) 1198.
- [9] R. R. P. Singh and J. Adler, *Phys. Rev.* **B54** (1996) 364; F. D. A. Aarao Reis, S. L. A. de Queiroz and R. R. dos Santos, *Phys. Rev.* **B60** (1999) 6740; A. Honecker, M. Picco and P. Pujol, *Phys. Rev. Lett.* **87** (2001) 047201; F. Merz and J. T. Chalker, *Phys. Rev.* **B65** (2002) 054425; N. Ito and Y. Ozeki, *Physica* **A321** (2003) 262; S. L. A. de Queiroz and R. Stinchcombe, *Phys. Rev.* **B68** (2003) 144414.
- [10] See e.g. R. B. Griffiths, "Rigorous Results and Theorems" in *Phase Transition and Critical Phenomena*, Vol. 1, edited by C. Domb and M. S. Green (Academic Press, London, 1972).
- [11] For recent results, see e.g. H. W. J. Blöte, L. N. Shchur and A. L. Talapov, *Int. J. Mod. Phys.* **C10** (1999) 1137; N. Ito, S. Fukushima, H. Watanabe and Y. Ozeki, "Recent Development in Nonequilibrium Relaxation Method" in *Computer Simulation Studies in Condensed-Matter Physics XIV*, edited by D. P. Landau, S. P. Lewis and H. -B. Schüttler (Springer-Verlag, Berlin, 2002); H. Arisue and T. Fujiwara, *Nucl. Phys. B* (Proc. Suppl.) **119** (2003) 855; *Phys. Rev.* **E67** (2003) 066109.